Sustainable Food Technology

ROYAL SOCIETY OF CHEMISTRY

PAPER

View Article Online
View Journal | View Issue

Cite this: *Sustainable Food Technol.*, 2026, **4**, 1898

Systematic investigation of metal–phenolic network-capped starch nanoparticles as sustainable coatings for postharvest fruit preservation

Tianyi Jin, Tianyu Wang, Sangeun Park, Danielle Morgan Schultze, Siyun Wang, Dangzhi Han and Tianxi Yang *

Sustainable coatings have emerged as an alternative for preserving fruit freshness and reducing food loss and waste. Metal–phenolic networks (MPNs) offer broad applicability in the agri-food sector by modifying food molecules and structures, and contribute to food preservation. This study systematically investigates the formation, characterization, and functional performance of a sustainable coating composed of MPN-capped-starch nanoparticles (MCS) using various combinations of metal ions (Fe^{3+}, Zn^{2+}) and polyphenols (tannic acid (TA) and epigallocatechin gallate (EGCG)) for postharvest fruit quality maintenance. The incorporation of starch nanoparticles (SNPs) effectively enhanced the barrier properties of MPN coatings by reducing gas exchange and water loss. Among the formulations, Fe–TA–MCS showed the strongest performance in limiting weight loss and maintaining firmness due to the dense network structure. Fe-based coatings also exhibited notable antimicrobial activity. Zn–EGCG–MCS was most effective in preserving surface color, titratable acidity, soluble solids, and phenolic content. Overall, Fe–TA and Zn–EGCG systems formed robust MPN crosslinks, and once capped onto SNPs, MPN-capped-starch nanoparticle formulations enable superior multifunctional performance in postharvest preservation compared with MPN formulations. This study provides a first demonstration and systematic analysis of the preservation performance of various MPN and MPN-formulated MCS coatings in grape preservation, offering insights for the future design and engineering of MPN systems customized for specific functional applications in food packaging and coating.

Received 1st November 2025
Accepted 22nd December 2025

DOI: 10.1039/d5fb00876j

rsc.li/susfoodtech

Sustainability spotlight

Postharvest fruit deterioration contributes significantly to global food waste and sustainability challenges. This study advances sustainable preservation by developing biodegradable coatings composed of metal–phenolic network (MPN)-capped starch nanoparticles (SNPs) that effectively reduce weight loss, microbial spoilage, and nutrient degradation while extending shelf life. Fe–tannic acid and Zn–epigallocatechin gallate systems form robust MPN crosslinks, and when integrated with SNPs, the resulting MPN-capped formulations exhibit superior multifunctional performance compared with conventional MPN coatings. This work supports the United Nations Sustainable Development Goals on Responsible Consumption and Production (SDG 12), Zero Hunger (SDG 2), and Good Health and Well-being (SDG 3) by minimizing food waste, enhancing food quality and safety, and promoting environmentally friendly materials for sustainable agri-food systems.

1 Introduction

Reducing food loss and waste is regarded as a key global strategy for balancing food systems and minimizing the associated environmental impacts.[1] The Food and Agriculture Organization of the United Nations (FAO) estimates that approximately one-third of all food produced globally is wasted each year. This issue is particularly severe for perishable commodities such as fruits and vegetables, where loss rates exceed 40%.[2,3] A central objective of the United Nations Sustainable Development Goals (SDGs) is to develop sustainable food processing technologies that ensure product safety while preserving quality and nutritional value.[4]

Sustainable coatings have emerged as an alternative for preserving fruit freshness. Once applied through dipping or spraying methods, these coatings can conform to the irregular shapes of various fruits and form an effective barrier against microbial contamination and oxygen exposure on the fruit surface.[2,5] Polysaccharides represent a major category of widely used biopolymers for sustainable coatings, owing to their biodegradability, environmental friendliness and safety. Among

Food, Nutrition and Health, Faculty of Land and Food Systems, The University of British Columbia, Vancouver V6T1Z4, Canada. E-mail: tianxi.yang@ubc.ca

them, starch has attracted increasing attention due to its low cost and abundant availability.[6,7] As a branched homo-polymer of glucose linked by α-1,4 linear and α-1,6 branched bonds, starch can be converted into starch nanoparticles (SNPs) through selective hydrolysis of its amorphous regions, resulting in nano-sized fragments with increased crystallinity.[8,9] Our previous research incorporated starch nanoparticles derived from mango seed waste into edible coatings, which significantly enhanced the sensory attributes and postharvest quality of tomatoes and kiwifruits.[10] Wang *et al.* developed a colorimetric, pH-responsive starch nanoparticle-based waterproof coating that exhibited excellent thermal stability and water repellency, attributed to a unique micro/nanostructure formed by stearic acid and starch nanoparticles.[11] In another study, pea starch nanoparticles infused with neem oil were employed as active coating agents to prolong the postharvest shelf life of strawberries.[12] Moreover, some small molecules can be loaded into starch nanoparticles during the process that starch molecules are rearranged by gelatinization and recrystallization, while the high surface area-to-mass ratio of starch nanoparticles provides abundant sites for surface modification, allowing for the attachment of functional groups.[11,13,14] These characteristic properties of starch nanoparticles enable their potential integration with antioxidant or antimicrobial agents for versatile edible coating applications.

Surface modification of SNPs offers significant potential to improve coating performance, with metal–phenolic networks (MPNs) emerging as a particularly promising nano-based approach. MPNs are amorphous structures formed through the coordination of polyphenolic ligands with metal ions, and can be rapidly assembled within minutes *via* polyphenol adsorption onto surfaces followed by metal-ion chelation to create stable, crosslinked coatings.[15–17] The functionalities of MPN composites show design flexibility, which can be engineered by selecting specific phenolic ligands and coordinating metal ions. Different combinations of metal and phenolic ligands result in metal-dependent properties of network and enable the expression of various biological activities inherent to polyphenols, such as antibacterial and anticancer effects.[15,18,19] MPNs offer broad applicability in the agri-food sector by modifying food molecules and structures and contribute to food preservation. They have been incorporated into various biopolymers, such as zein, soy protein, and starch, to enhance structural and functional properties.[20–23] The rapid film-forming properties and synergistic antibacterial and antioxidant effects have also been revealed in developing sprayable coating solutions and enhancement of polymer matrix-based packing films.[18,24–26] However, current research primarily focuses on applying individual types of MPNs, with limited systematic studies comparing different combinations of phenolic ligands and metal ions and evaluating their relative effectiveness in food preservation. Furthermore, the functionalization of starch nanoparticles with MPNs for such applications remains largely unexplored.

We aim to develop sustainable coatings based on diverse compositions of MPNs and MPN-capped starch nanoparticles (MCS) and systematically evaluate their postharvest preservation effects on fresh produce. MPNs were synthesized *via* a self-assembly method to form a network structure using common dietary metal ions (Fe^{3+}, Zn^{2+}) and polyphenolic compounds (*e.g.*, tannic acid (TA) and epigallocatechin gallate (EGCG)), known for their significant health benefits. Characterization was conducted to analyze and compare the microstructural and chemical properties of these nanoparticles. MCS were prepared by capping different compositions of MPNs, including Zn–EGCG, Zn–TA, Fe–EGCG and Fe–TA, onto SNPs by self-assembly. Grapes, one of the most widely consumed fruits in the world, are selected as a model of fruit. Grapes are known for their desirable flavor and are an excellent source of nutrient compounds and natural antioxidants.[27] Fresh grapes are highly perishable and sensitive to temperature and moisture, resulting in a short shelf life after harvesting due to texture deterioration, dehydration, and high softening and respiration rates.[28,29] To reduce postharvest losses in grapes, preservatives such as sulfur dioxide are commonly used to inhibit microbial growth and oxidative spoilage.[30,31] However, residues of these chemicals raise health concerns for consumers. In our study, the effectiveness of the coatings in maintaining grape freshness during postharvest storage is assessed using several quality indicators, including color and visual appearance, weight loss, firmness, titratable acidity, total soluble solids, and total phenolic content. This study provides a systematic investigation of various MPN and MCS formulations, highlighting that distinct combinations of metal ions and polyphenols modulate the functional performance in sustainable coating systems.

2 Materials and methods

2.1 Materials

Tannic acid (ACS reagent, ≥99%), epigallocatechin gallate, iron(III) chloride hexahydrate ($FeCl_3 \cdot 6H_2O$), zinc chloride($ZnCl_2$, reagent grade, ≥98%), and other reagents were purchased from Sigma-Aldrich. Native corn starch was purchased from Bob's Red Mill (Canada). Folin & Ciocalteu's phenol reagent (2 M, with respect to acid) were obtained from Fisher Scientific. Table grapes (green seedless grape) were purchased at a local supermarket (Save-on-Foods, Vancouver, Canada). All other reagents used were of analytical grade.

2.2 Preparation and characterization of coating solutions

The method for preparing MCS was adapted from the approach described by Qin *et al.*[32] The synthesis of SNPs was achieved by acid hydrolysis. Fifteen grams of native corn starch were dispersed in 100 mL of 3.16 M sulfuric acid at 40 °C with continuous stirring at 150 rpm for 7 days. After hydrolysis, the aqueous suspension was washed in distilled water by centrifugation (10000 rpm for 5 min) until neutrality was reached. After neutralization, the precipitated starch hydrolysate was dispersed in acetone for solvent replacement by washing three times with acetone and centrifugation (25000 rpm for 5 min). The SNP suspension was dried in an air oven at 40 °C for 12 h. Starch nanoparticles (250 mg) were dispersed in 24.5 mL of deionized water. Polyphenolic acid (tannic acid (TA) and

epigallocatechin gallate (EGCG)) and metal ions (Fe^{3+}, Zn^{2+}) were gradually added to the nanoparticle suspension in alternating 10 μL aliquots. A total of 250 μL of polyphenolic acid (25 mM) and 250 μL of metal ions (Fe^{3+}, Zn^{2+}) (50 mM) were added. The suspension was sonicated in an ultrasonic bath at a frequency of 45 kHz for 15 s immediately following each individual addition of polyphenolic acid and the metal ions. The solution was placed for 1 h for assembly of the MPN. The aqueous suspension was washed three times in deionized water to remove excess polyphenolic acid and metal ions (25000 rpm for 3 min). Scanning electron microscopy (SEM, Merlin, Zeiss) was used to characterize the micro-morphology of the samples. The dispersions were not diluted before starting the measurements. Dynamic light scattering (DLS) was used to measure particle diameters with a Malvern Nano-Zetasizer Instrument at 25 °C. Fourier transform infrared (FTIR) spectra of SNPs and FTN@SNPs were collected using a Fourier Transform Infrared Spectrometer (Nicolet IS50, Thermo Fisher Scientific, USA). Each measurement was performed in triplicate and the values were averaged to obtain the mean particle size.

2.3 Fruit sample selection and coating dipping

Coatings on fruit were applied according to a previous research method with adaptations.[33] The grapes were grouped according to 3 different coating treatments and postharvest quality measurement days (0, 3, 6, 9, 12, 15 days) with 3 replicates for each condition. Each sample group contained 5 fruits with a clean surface, uniform shape and maturity. The grapes were then dipped in the different coating formulations and placed on a support to dry for 2 h under ambient laboratory conditions (20 °C). The grapes (both coated and uncoated) were stored in open trays to simulate exposure to external factors (light, oxygen, temperature), closely resembling postharvest and commercial conditions (Fig. S1). All grapes were stored at 20 °C for 15 days. The relevant physiological and chemical indexes of all groups were measured and recorded every 3 days.

2.4 Color and visual appearance

The color of the treated and control grapes was measured based on the CIE $L^*a^*b^*$ tristimulus color parameters' (L^*, lightness/darkness; a^*, red/green; and b^*, blue/yellow) coordinates. Color of the samples was recorded using a colorimeter (HunterLab, model LabScanTM XE Plus, Hunter Associates Laboratory, Reston, VA, USA). Measurements were carried out at four equidistant positions on the surface of each grape, using five grapes, and the mean values were reported. The total color difference (ΔE) was calculated for all samples using the following equation:[34]

$$\Delta E = \sqrt{(\Delta L)^2 + (\Delta a)^2 + (\Delta b)^2}$$

Grapes were photographed using a digital camera to monitor changes in appearance on day 0 and every 3 days for up to 15 days. The same angles and light were controlled for all photographic documentation using a photo studio lightbox (SLOW DOLPHIN, Canada). Principal Component Analysis (PCA) was performed on a standard RGB image captured using MATLAB. The image, consisting of 3 color channels (Red, Green, and Blue), was reshaped into a 2D matrix where each row represented a pixel and each column represented one of the color channels.[35] PCA was then applied to this matrix to identify the principal components.

2.5 Weight loss and fruit firmness

Weight loss of grapes during storage showed the percentage loss of the initial weight. Weight loss was determined by measurements from 5 samples on days 3, 6, 9, 12 and 15. The fruit weight loss (%) was determined according to the following equation:

$$\text{Weightloss}(\%) = \frac{x - y}{x} \times 100$$

where x is the initial weight at the start of the storage, and y is the weight on the inspection date or the final weight.

The firmness of the grapes was assessed using a Texture Analyzer (TA-XT plus, SMS, UK) by utilizing a P/25 cylindrical probe with a constant speed of 2.0 mm s^{-1} to a deformation of 25%. A total of three replicate groups, each containing eight grapes, were analyzed. The results were reported as mean values in Newtons (N).

2.6 Determination of total soluble solids, titratable acidity and total polyphenolic content

The sample (10 g) was homogenized with 100 mL water using a blender (LINKChef, Canada) followed by centrifugation (5000 rpm, 3 min) to separate the pulp and the juice. Total soluble solids were measured using a hand-held refractometer (Mettler Toledo, RE50 Refractometer, USA). The instrument was first calibrated using distilled water before the test. Subsequently, 0.5 mL of each juice sample was loaded onto the refractometer individually to obtain readings, which were expressed as °Brix.

The titratable acidity was measured according to the method described by Chetia *et al.*[36] Titratable acidity was determined by titration of grape juice with 0.1 N NaOH solution until the end of titration (pH 8.1). The volume of NaOH was converted to grams of tartaric acid per 100 mL of juice, and TA was calculated using the following equation:

$$\text{Tannic acid} = \frac{V \times 0.1\ \text{N}\ \ \text{NaOH} \times 0.075 \times 100}{V_0}$$

where V is the volume (mL) of NaOH and V_0 is the volume of grape juice.

Total phenolic content (TPC) of the samples was determined using the Folin–Ciocalteu method, with modifications based on previous research.[37] To extract, 1 g of peeled grape pulp was added to 5 mL of 1% hydrochloric acid methanol solution and extracted in an ice bath for 5 min. Then, the reaction solution was centrifuged at 4000 rpm for 10 min, and the supernatant was diluted to an appropriate concentration for further measurements. Each extract (20 μl) was added into tubes, and 1.58 mL of distilled water was added. A total of 100 μl of Folin–

Ciocalteu reagent (diluted 1 : 10 ratio with distilled water) was added and immediately mixed. After waiting for 8 min, 300 μl of sodium carbonate solution [7.5% (w/v) in distilled water] was added and mixed. Then, the solutions were incubated in a dark place for 2 h at room temperature. The absorbance of each solution was measured at 765 nm with a spectrophotometer (Infinite M200 pro microplate spectrofluorophotometer, Tecan, Switzerland). The TPC of samples was calculated as mg gallic acid equivalent (GAE) per kg fresh fruit by using a standard curve of gallic acid.

2.7 Characterization of antioxidant and antimicrobial properties of different coating solutions

The antioxidant activity of the coating was evaluated through DPPH radical scavenging on a 96-well microplate, according to the methodology described in a previous study.[38] DPPH (2,2-diphenyl-1-picrylhydrazyl) was solubilized in ethanol to prepare a solution and was stored in amber glass to prevent light. One hundred μL of each washing solution was mixed with 3.9 mL of DPPH solution (25 mM) and added to each well. The solutions were incubated for 45 min at room temperature in the dark. The absorbance was measured at 517 nm against water as a blank using a fluorescence spectrophotometer (Tecan infinite 200Pro plate reader). The DPPH radical scavenging activity of each coating was calculated using the following equation:

$$\text{DPPH radical scavenging activity} = \frac{A_0 - A_1}{A_0} \times 100\%$$

where A_0 is the absorbance of the DPPH solution at 517 nm, A_1 is the absorbance of DPPH and the coating mixture at 517 nm after incubation.

The ABTS radical scavenging assay was performed according to the method described in a previous study.[39] A concentrated ABTS solution was prepared by dissolving 2,2-azinobis-(3-ethylbenzothiazoline-6-sulfonic acid) (ABTS) and potassium persulfate ($K_2S_2O_8$) to achieve a final concentration of 140 μmol L^{-1} (pH = 7.4). The mixture was incubated in the dark at room temperature to generate the ABTS radical. The ABTS radical solution was then diluted with distilled water to achieve an absorbance of 0.70 ± 0.02 at 734 nm. Subsequently, 1 mL of this ABTS solution was mixed with 1 mL of the sample solutions. Deionized water was used as the blank control in the experiment. After incubating the samples in the dark for 8 min at ambient temperature, their absorbance values were measured at 734 nm. ABTS radical scavenging activity was calculated using the following equation:

$$\text{ABTS radical scavenging activity} = \frac{B_0 - B_1}{B_0} \times 100\%$$

where B_0 represents the absorbance of the ABTS solution measured at 734 nm, while B_1 means the absorbance of the reaction mixture at 734 nm, after a 30-min reaction period.

The antimicrobial activity of the different MCS solutions (Fe-EGCG-MCS, Fe–TA–MCS, Zn–EGCG–MCS; Zn–TA–MCS) against *Staphylococcus epidermidis* ATCC 12228 was determined by the agar disk diffusion method. *S. epidermidis* was cultured in Tryptic Soy Broth (TSB) medium and grown aerobically at 37 °C for 24 at 150 rpm in a shaking incubator. The suspension was centrifuged (8000 rpm, 4 °C, 5–10 min) and washed with PBS (Phosphate-Buffered Saline) 3 times. Subsequently, the microbial suspension was diluted with PBS to obtain 10^8 colony forming units (CFU) per mL suspensions, with OD_{600} values of 0.5, and further diluted into 10^7 CFU mL^{-1} and 10^6 CFU mL^{-1}. Two hundred microliters (200 μL) of each diluted microbial suspension were incubated with equal volumes of coating solutions for 30 min and then uniformly spread on tryptic soy agar (TSA) plates (Avantor, Canada). The plates were incubated overnight at 37 °C, and colony counts were recorded the following day along with images of the corresponding plates.

2.8 Data analysis

All data are presented as mean ± standard deviation from 5 independent replicates. One-way ANOVA followed by Turkey's multiple range test was conducted to evaluate significant differences among treatments at a 5% significance level ($p < 0.05$). Superscript letters (a, b, c, d) indicate statistical groupings from Tukey's test; groups sharing a letter are not significantly different ($p > 0.05$) (Table S1–S7). Statistical analyses and data visualization were performed using GraphPad Prism 9.

3 Results

3.1 Characteristics of metal–phenolic network-capped starch nanoparticles (MCS)

Metal phenolic networks can be formed on a starch-based matrix through self-assembly. SNPs can first associate with two phenolic acids *via* different mechanisms: TA formed layers through molecule diffusion and attracted galloyl and catechol groups on starch particles;[21] whereas (−)-epigallocatechin gallate (EGCG) was conjugated onto starch by an acid-mediated coupling method.[40] After introducing metal ions (Fe^{3+}, Zn^{2+}) to SNP–phenolic complexes, MPNs are formed through metal–ligand coordination, creating layer-by-layer hierarchical 3D nanoarchitectures. Furthermore, the difference of the MPN structure could affect the MCS coating properties for preservation (Fig. S2).[41] As shown in Fig. 1a, the addition of Fe^{3+} to the SNP–phenolic complex resulted in a color change of the mixed solutions from clear to dark blue, whereas the addition of Zn^{2+} resulted in a white colloidal appearance of solutions. To further confirm the presence of the MPN in the SNP complex, FTIR spectroscopy was applied to determine interactions between the chemical components (Fig. 1b). All four metal–phenolic coated SNP complexes (MCS) exhibited overall spectral profiles that remained broadly consistent with the SNP baseline, including characteristic peaks around 2930 cm^{-1}. The FTIR spectrum of SNPs showed a broad absorption band at 3307 cm^{-1}, corresponding to O–H stretching vibrations. The increased intensity of this peak following MPN modification suggests enhanced hydrogen bonding, likely due to the interaction between polyphenol ligands and hydroxyl groups on the starch surface. In the EGCG-modified systems, new peaks emerged at 1614 cm^{-1} (C═O stretching) and 1690 cm^{-1} (aromatic C═C stretching), which were consistent with the presence of galloyl and catechol

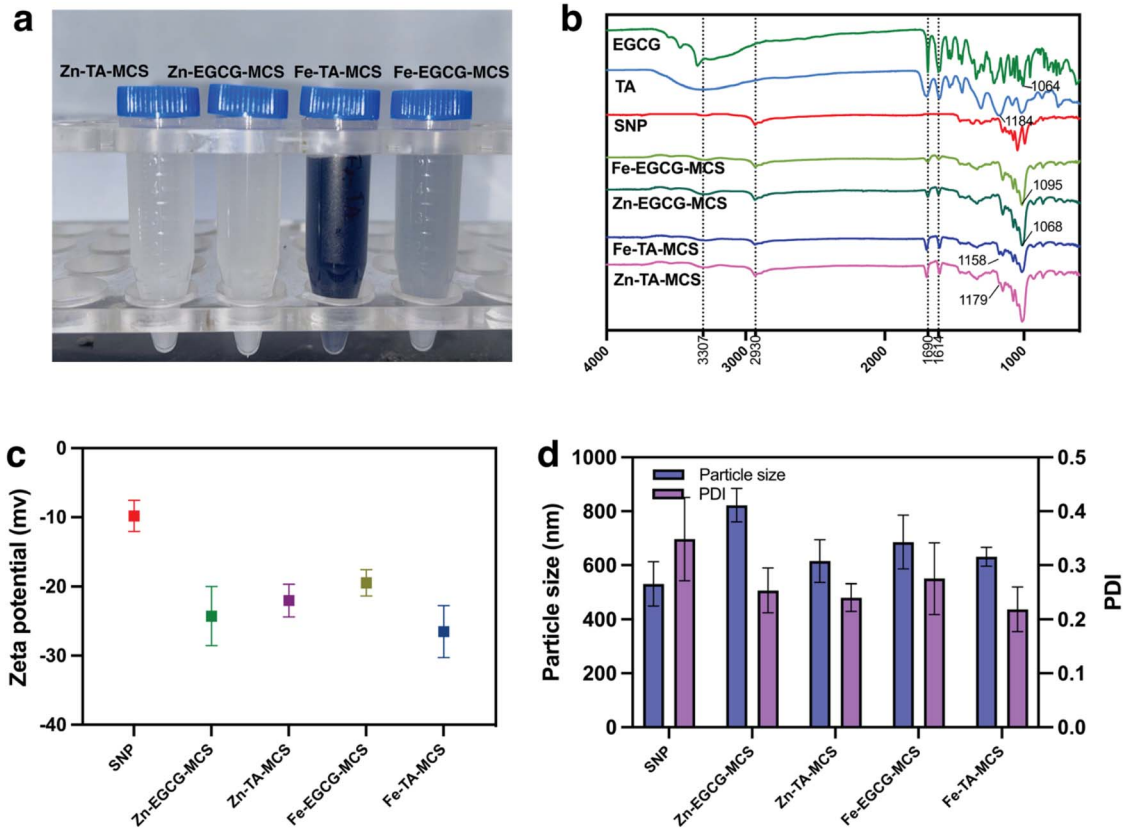

Fig. 1 (a) Formulation of four metal–phenolic-network capped starch nanoparticles (MCS); (b) Fourier-transform infrared (FTIR) spectra; (c) zeta potential (pH = 4); (d) dynamic light-scattering analysis.

functionalities. The C–O stretching band at 1064 cm^{-1} shifted to 1095 cm^{-1} in the Fe–EGCG–MCS, suggesting strong coordination between Fe^{3+} and phenolic groups; while a more modest shift to 1068 cm^{-1} was observed in the Zn–EGCG–MCS. Similarly, the TA-coated SNPs showed characteristic new bands at 1607 and 1699 cm^{-1}, corresponding to aromatic C–O, C=C stretching, and carbonyl groups, respectively. The C–O band at 1184 cm^{-1} shifted to 1158 cm^{-1} in the Fe–TA–MCS, indicative of potential Fe–TA coordination, while a minor shift to 1179 cm^{-1} occurred in the Zn–TA–MCS.

Furthermore, synthesized MPN capped SNPs were characterized based on zeta potential (Fig. 1c), and the polydispersity index (PDI) and average particle size (Fig. 1d). The PDI was measured to reveal the uniformity of nanoparticles. When the PDI is below 0.30, the sample is considered to have a relatively narrow and uniform size range.[42] Coating SNPs with the MPN substantially enhanced their colloidal stability compared with bare particles ($p < 0.05$), with all coated formulations exhibiting PDI below 0.30. Dynamic light-scattering analysis revealed that mean hydrodynamic diameters of Zn–TA–MCS, Fe–EGCG–MCS and Fe–TA–MCS were 615.47 ± 79.31, 685.76 ± 99.53, and 631.33 ± 35.26 nm, respectively. The observed increases relative to the bare SNPs (531.26 ± 81.3 nm) indicate successful coating with the MPN. Notably, Zn–EGCG–MCS exhibited markedly greater dimensions (822.24 ± 62.18 nm) compared to all other MCS, potentially attributable to the distinct mesoporous architecture of Zn–EGCG–MPN.[43] Zn–TA–MCS presented smaller particle sizes than Fe–TA–MCS, which was consistent with previous research in which TA/Zn-MPN formed an interfacial adsorption layer 3 times denser than that of TA/Fe-MPN.[44] For both metal types, EGCG-based MCS demonstrated larger particle sizes compared to TA-based MCS, likely due to differences in the polyphenol coordination mechanisms to SNPs. The zeta potentials of all MCS were measured at pH 4. The results ranged from −19.47 ± 1.89 to −26.51 ± 3.77 mV, notably more negative than that of the bare SNPs (−9.81 ± 2.25 mV), further confirming successful MPN coating. According to previous findings,[45] nanoparticles with zeta potential values in the range of ±20 to ±40 mV possessed moderate colloidal stability due to sufficient electrostatic repulsive forces. The increased negative charge imparted by the MPN coating effectively enhances electrostatic repulsion, consequently reducing nanoparticle aggregation.

3.2 Weight loss and firmness

The weight loss of all groups of grapes is shown in Fig. 2a and Table S1. When compared with the control group, all coating treatments demonstrated improved preservation in terms of weight loss. Overall, MCS coatings exhibited superior performance compared to the MPN coatings. This finding indicates the effectiveness of starch nanoparticles in forming a protective barrier that minimizes gas exchange, thereby preserving firmness and reducing weight loss. Previous studies have reported

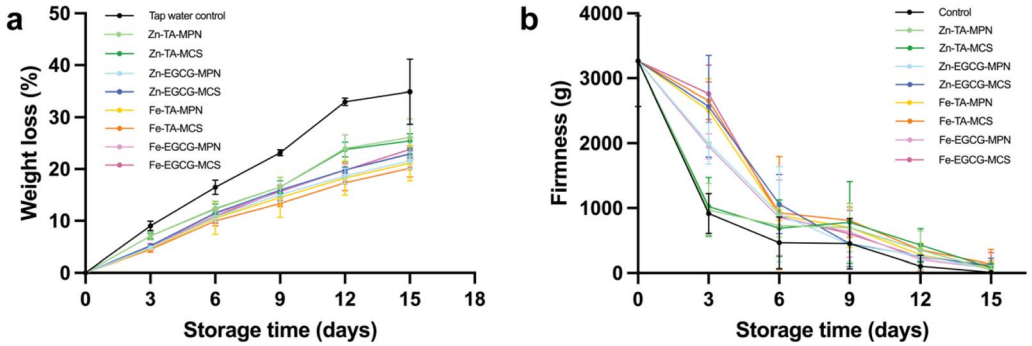

Fig. 2 (a) Weight loss and (b) firmness of different MPN and MCS coated groups and the control group.

this beneficial function of starch-based fruit coatings.[10,46] Fe–TA–MCS exhibited the most markedly protective effect in reducing weight loss throughout storage, closely followed by Fe–TA–MPN. The effectiveness of Fe–TA based coatings in limiting weight loss can likely be attributed to their compact crosslinked structure, resulting in a dense network that effectively prevents moisture evaporation and gas exchange.[47] Conversely, Zn–TA based coatings demonstrated limited effectiveness in reducing weight loss.

Fruit firmness is another critical factor reflecting the post-harvest quality changes and it strongly influences the consumer acceptance.[48,49] Changes in the firmness of control and treated grapes over storage time are shown in Fig. 2b and Table S2. Within the first 6 days of storage, Zn–EGCG–MCS and Fe–TA–MCS showed superior results in maintaining firmness, while grapes treated with Zn–TA based coatings demonstrated the lowest firmness values among all the coated treatments. The coating type did not significantly affect the firmness of grapes after 15 days of storage ($p > 0.05$). At the end of the storage period, firmness loss of coated grapes was in the range of 50–80 g, whereas that of control grapes was about 10 g of firmness.

3.3 Color and visual appearance

Table S3 shows the surface color changes of different coated and uncoated grapes stored for 15 days. Uncoated control grapes demonstrated a significant decline in L^* (lightness), an

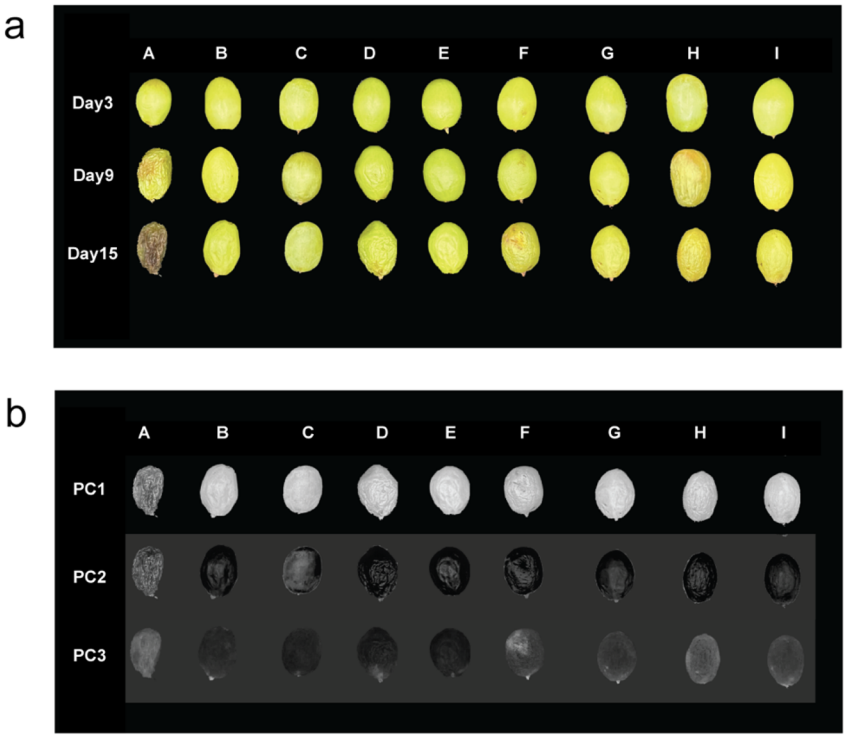

Fig. 3 (a) Representative images showing the visual appearance of grapes under different coating treatments during storage on day 3, day 9, and day 15. (b) Principal Component Analysis (PCA) applied to day-15 grape images. The first three principal components (PC1, PC2, and PC3) are listed, showing the dominant patterns of variation in surface color distribution, texture contrast, and shrinkage shading across different coating treatments. Treatments include: (A) uncoated control, (B) Zn–EGCG–MPN, (C) Zn–EGCG–MCS, (D) Zn–TA–MPN, (E) Zn–TA–MCS, (F) Fe–EGCG–MPN, (G) Fe–EGCG–MCS, (H) Fe–TA–MPN, and (I) Fe–TA–MCS.

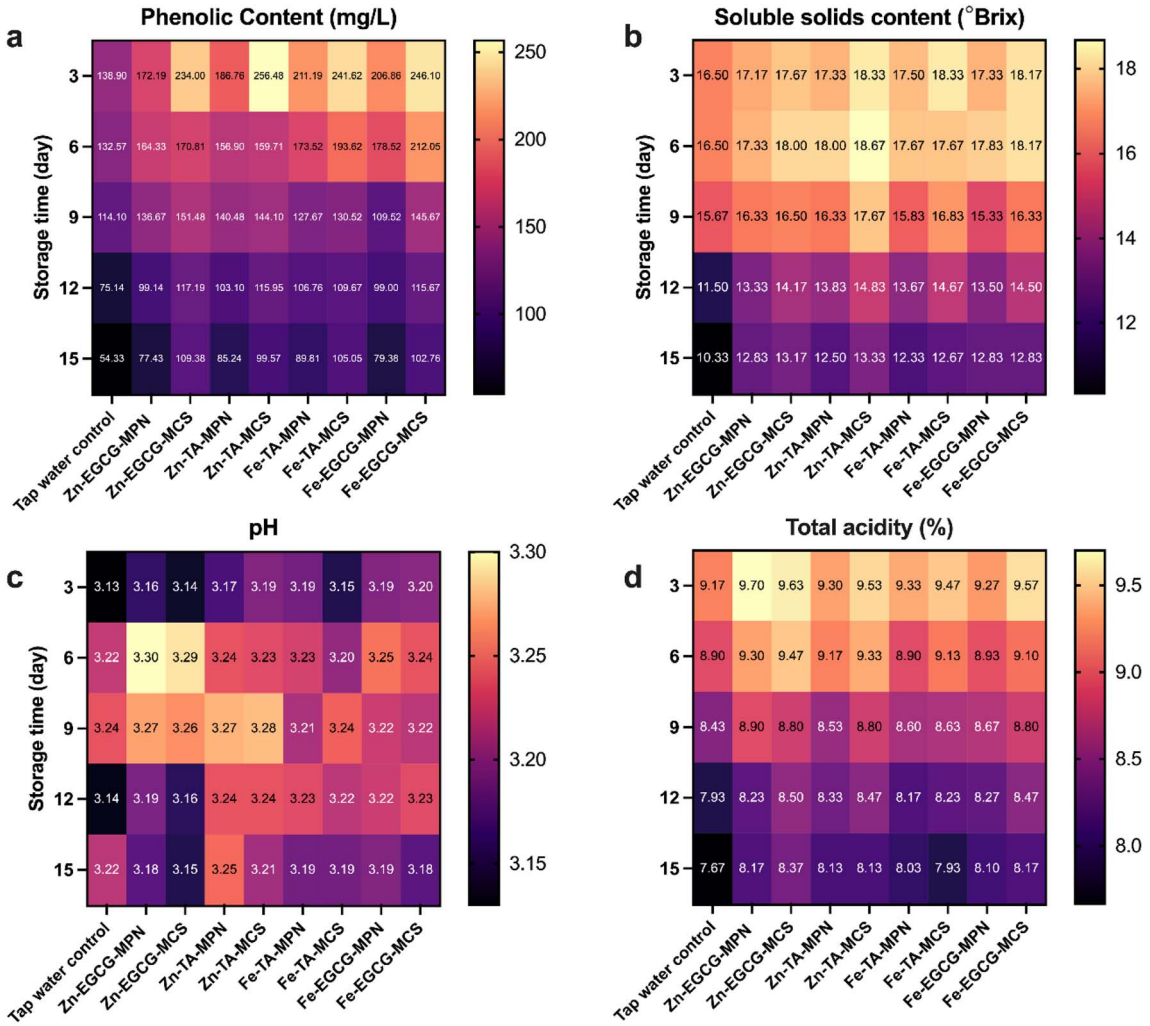

Fig. 4 Grape preservation experiment results. Changes in (a) total phenolic content, (b) total soluble solid content, (c) pH and (d) total acidity of the grapes during 15 days of storage.

increase in a^* (shifting towards a greener hue), and an increase in b^* (indicating increased yellowness), consistent with the progression of browning. By day 3, there was a slight, non-significant decrease ($p > 0.05$) in b^* values observed in Fe-coated grapes, which may be attributable in part to the intrinsic blue coloration of the Fe-containing coating solutions but it does not exert a detrimental effect on the overall color quality of the product. Notably, on day 15, Zn-based coatings proved more effective than Fe-based coatings in preserving higher L^* values and mitigating the green shift (a^*). These results aligned with prior research which reported that ZnO coatings inhibited browning by attenuating oxidative stress and pigment degradation.[50] MCS-based coatings maintained higher L^* values compared to their equivalently composited MPN groups, likely due to the formation of enhanced barrier layers by starch nanoparticles, which restricted oxygen contact with the fruit surface. It was determined that the specific type of polyphenol that was incorporated within the MPN and MCS formulations did not induce statistically significant differences in L^*, a^*, and b^* values on day 15 ($p > 0.05$).

Fig. 3a and S3 present the morphological changes of grapes from day 3 to day 15 after different coating treatments. To quantitatively distinguish these variations, Principal Component Analysis (PCA) was conducted on day 15 grape images (Fig. 3b). PCA is a statistical tool that represents data using uncorrelated variables named principal components (PC) instead of original variables which are possibly correlated.[35] As shown in Fig. 3b, the higher-order principal components (PC3) clearly differentiated grapes coated with Zn-based formulations (B–E) from the control group (A). The coated grapes exhibited notable visual differences attributed to the comprehensive effectiveness of Zn-based coatings in diminishing browning and preserving color, minimizing wrinkles, and reducing dehydration on day 15.

3.4 Titratable acidity, total soluble solids and total phenolic content

During the 15 days of storage, various parameters of postharvest quality were measured, including titratable acidity, pH, total soluble solids, and total polyphenolic content, and the results

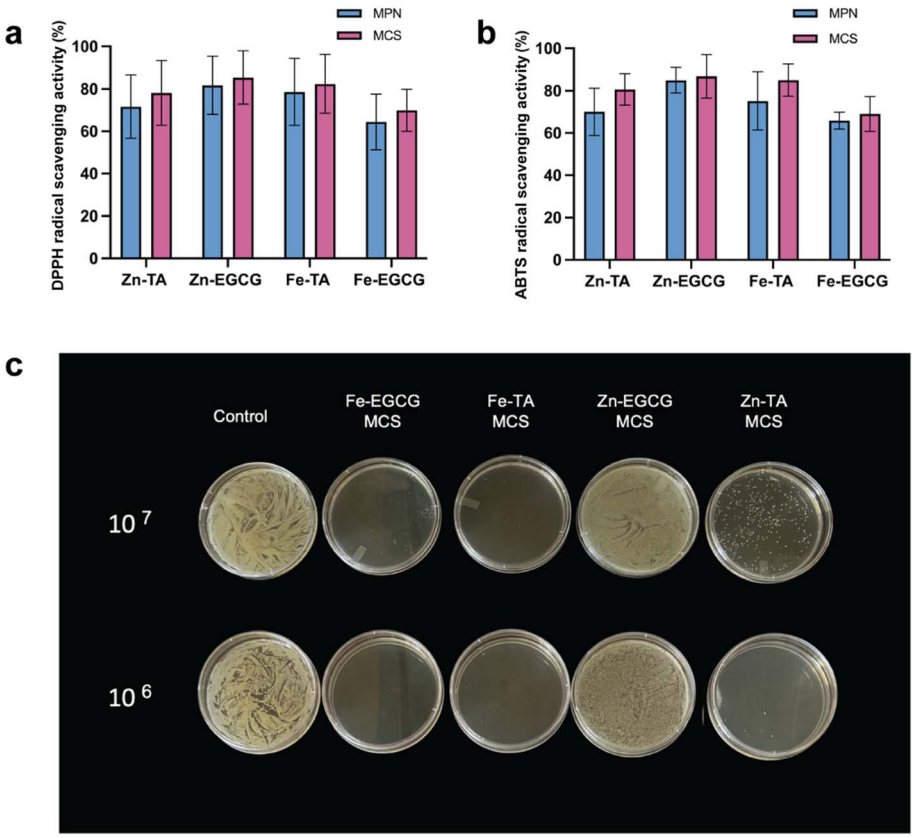

Fig. 5 Antioxidant and antibacterial properties of the MCS composite coating solutions: (a) DPPH and (b) ABTS radical scavenging activities. (c) *S. epidermidis* plate images.

are presented as heatmaps in Fig. 4. The total phenolic content in grapes gradually declined throughout the storage period (Fig. 4a and Table S4). However, grapes coated with MCS/MPN composite solutions retained higher phenolic levels after 15 days compared to the control group. Among all treatments, the Zn–EGCG–MCS coating resulted in the highest retention of the phenolic content, with 109.38 mg L^{-1}. Changes in °Brix values of different grapes are illustrated in Fig. 4b and Table S5. The ° Brix of all samples decreased over time, but notably higher levels were observed in grapes treated with Zn–TA–MCS (13.33 ° Brix) and Zn–EGCG–MCS (13.17 °Brix) on day 15. The observed decrease in total soluble solids during storage may be attributed to several factors, including the extent to which water loss exceeds the decomposition of sugars and other soluble components.[50] There were no significant differences in pH among the groups, with values fluctuating between 3.1 and 3.3 (Fig. 4c and Table S6). While pH measures the concentration of free hydrogen ions (H^+) and reflects the immediate acidity or alkalinity of a solution, titratable acidity represents the total amount of proton-donating acids present, which is a more comprehensive indicator of the acid content and is closely related to taste and freshness.[51,52] The Zn–EGCG–MCS coating was more effective in preserving total titratable acidity, with a retention rate of 8.37% (Fig. 4d and Table S7). Overall, Zn–EGCG–MCS showed the best performance in maintaining postharvest quality. It exhibited strong oxygen barrier and antioxidant properties, which limited respiration and oxidative reactions, thereby slowing down metabolic processes such as auto-respiratory activity and the hydrolysis of monosaccharides in the grape.[49,53] As a result, the degradation of bioactive compounds and ascorbic acid was substantially delayed, thus contributing to the preservation of overall fruit quality during storage.

3.5 Assay of antioxidant and antimicrobial properties

The phenolic hydroxyl groups present in polyphenols significantly contribute to their antioxidant activities both *in vitro* and *in vivo*, making them widely applicable in fields including food packaging.[54] A previous study demonstrated that metal ions retained their oxidation states within the MPN matrix after incorporation, consequently enhancing the antioxidant capacity of the system.[55] In this study, the antioxidant capacities of different compositions of MPNs before and after grafting SNPs into the system were evaluated by DPPH radical scavenging capacity and ABTS radical scavenging capacity (Fig. 5a and b).

DPPH is a relatively stable free radical characterized by a strong absorption peak at 517 nm; upon interaction with free radical scavengers or hydrogen-donating substances, it is converted to diphenylpicrylhydrazine, which does not absorb at this wavelength.[56] Fig. 5a shows the scavenging activity of four different compositions of MPNs and MCS against a 25 mM DPPH solution. The original MPN showed a certain extent of

DPPH radical scavenging activity; however, it was slightly enhanced by complexation with SNPs. This phenomenon was also observed in an ABTS free radical scavenging experiment. Similarly, studies which incorporated other polysaccharides such as chitosan reported that intermolecular hydrogen bonds made the system more sensitive to DPPH radicals.[26,57] Zn–EGCG–MCS and Fe–TA–MCS demonstrated substantial antioxidant performance among all coating compositions, achieving DPPH radical scavenging efficiencies of 85.39% and 82.41%, respectively. Zn–TA–MCS exhibited a relatively lower performance at 78.12%, whereas Fe–EGCG–MCS showed the lowest capacity at 69.97%. The results obtained from the ABTS assay shown in Fig. 5b further validate this ranking. The differences observed in antioxidant capacity among the MPN group and MCS compositions group were likely due to coordination effects. Apart from the original antioxidant properties of polyphenols, the introduction of metal ions enhanced antioxidant performance by shifting electron density from the aromatic rings toward the metal ions, consequently lowering the energy required for hydroxyl group dissociation. Furthermore, the extent of electron redistribution within the aromatic rings of phenolic compounds significantly varied depending on the coordinated metal ion, generally increasing with the radius of metal ions.[58,59] This suggests a coordination-dependent mechanism underlying the antioxidant performance.

The antimicrobial efficacy of the MCS coatings appears to be primarily dependent on the metal instead of the type of polyphenol ligand. *Staphylococcus epidermidis* (ATCC 12228) is a Gram-positive bacterium classified among foodborne pathogens.[60] Owing to its safety and physiological similarity, *S. epidermidis* is frequently employed as a surrogate for the pathogenic coagulase-positive *Staphylococcus aureus* in both clinical and food studies.[61] It serves as a suitable model for evaluating the antimicrobial activity of functional edible ingredients, such as essential oils, and the effectiveness of antimicrobial food packaging films.[60,62] This is evident from the *S. epidermidis* growth patterns observed at both concentrations (10^7 and 10^6 CFU mL^{-1}) in Fig. 5c (colony enumeration in Table S8 and full representative plates in Fig. S4). The antimicrobial efficacy of the MCS coatings appeared to be metal ion-dependent rather than dependent on the type of polyphenol ligand. This is evident from the *S. epidermidis* growth patterns observed at both concentrations (10^{-7} and 10^{-6} CFU mL^{-1}) in Fig. 5c and S4. At both concentrations, Fe-based MCS coatings demonstrated a strong and consistent antibacterial effect, as indicated by the complete inhibition of bacterial colony formation below the detection limit. In contrast, Zn-based MCS coatings showed incomplete inhibition, with visible bacterial growth—particularly in Zn-TA MCS, which exhibited the highest bacterial concentration among all tested coatings. This consistent performance across two bacterial concentrations supports the interpretation that the metal ion played a dominant role in antimicrobial effectiveness. Fe-coordinated systems may exhibit enhanced antimicrobial activity due to multiple mechanisms: radicals may disrupt bacterial membranes and damage essential cellular components (*e.g.* DNA and enzymes), while metal redox cycling can deplete cellular antioxidants, collectively leading to bacterial cell death.[63,64] These effects likely contribute to the superior antimicrobial performance observed in Fe-based MCS systems.[65,66]

4 Final considerations

In this study, all MPN and MCS formulations showed measurable effectiveness in preserving grape quality compared with the uncoated control. Incorporation of SNPs enhanced barrier properties, reduced gas exchange, and improved antioxidant capacity through hydrogen bonding with polyphenolic ligands. Among all treatments, Fe–TA–MCS most effectively minimized weight loss and maintained firmness, likely due to its compact network structure, while Zn–EGCG–MCS better preserved surface color, acidity, soluble solids, and phenolic content. The superior performance of Zn–EGCG–MCS was attributed to Zn^{2+}'s regulation of enzymatic pathways and its strong coordination with EGCG. Overall, Fe–TA and Zn–EGCG coatings formed robust networks, enabling multifunctional postharvest preservation. Based on the quality indices evaluated, these metal-phenolic-formulated coatings extended the shelf-life of grapes from approximately 9 days for the uncoated control to at least 15 days. Future studies can focus on exploring the role of multiple metal and phenolic ligands (co-coordination effects and identifying potential synergies) and MPN/SNP ratios to enable large-scale application and evaluate the nutritional value and potential health effects of these coatings. In addition, the potential sensory impact and regulatory limits should be investigated across diverse fruit and vegetable commodities. This study showed the first demonstration and systematically evaluated the preservation performance of various MPN and MCS coatings on grape quality, which offers guidance for designing and engineering MPN systems tailored to targeted functions in food packaging and coating applications.

Author contributions

Tianyi Jin: original draft writing, methodology, investigation, formal analysis. Tianyu Wang: investigation, formal analysis. Sangeun Park: investigation, formal analysis. Danielle Morgan Schultze: review and editing. Siyun Wang: review and editing. Dangzhi Han: investigation, formal analysis. Tianxi Yang: conceptualization, review and editing, supervision, funding acquisition. All authors have read and agreed to the published version of the manuscript.

Conflicts of interest

The authors declare no known conflict of interest.

Abbreviation

DLS	Dynamic light scattering
EGCG	Epigallocatechin gallate
FTIR	Fourier transform infrared
MPN	Metal–phenolic networks

MCS	MPN-capped-starch nanoparticles
PCA	Principal Component Analysis
SNPs	Starch nanoparticles
TA	Tannic acid

Data availability

Data will be made available upon request from the corresponding author.

Supplementary information (SI): figure showing: scanning electron microscopy (SEM) images of 4 MPNs (Fig. S1); schematic illustration of grape pre-processing and dipping–coating procedures (Fig. S2); visual appearance of grapes over 15 days of storage (Fig. S3); antibacterial properties of MCS composite coating solutions (Fig. S4); weight loss of grapes (Table S1); firmness of grapes (Table S2); color indexes of different grape sample groups (Table S3); total phenolic content of grapes (Table S4); total soluble solid of grapes (Table S5) subjected to different treatments during 15 days of storage. pH of grapes (Table S6); total acidity of grapes (Table S7); colony enumeration of *S. epidermidis* (Table S8). See DOI: https://doi.org/10.1039/d5fb00876j.

Acknowledgements

The authors acknowledge the UBC Bioimaging Facility (RRID: SCR_021304) for providing access to scanning electron microscopy resources used in this study. This work was supported by the UBC Faculty of Land and Food Systems/Start Up Funds (AWD-020249 UBCLANDF 2022), Natural Sciences and Engineering Research Council of Canada (NSERC) Discovery Grants Program (RGPIN-2023-04100) and NSERC Discovery Grants Program-Discovery Launch Supplement (DGECR-2023-00386). We acknowledge the Canada Foundation for Innovation and John R. Evans Leaders Fund (CFI-JELF #44768), and the British Columbia Knowledge Development Fund (BCKDF).

References

1 M. Springmann, M. Clark, D. Mason-D'Croz, K. Wiebe, B. L. Bodirsky, L. Lassaletta, W. de Vries, S. J. Vermeulen, M. Herrero, K. M. Carlson, M. Jonell, M. Troell, F. DeClerck, L. J. Gordon, R. Zurayk, P. Scarborough, M. Rayner, B. Loken, J. Fanzo, H. C. J. Godfray, D. Tilman, J. Rockström and W. Willett, *Nature*, 2018, **562**, 519–525.
2 Y. Cui, Y. Cheng, Z. Xu, B. Li, W. Tian and J. Zhang, *Adv. Sci.*, 2024, **11**, 2409560.
3 S. L. R. García and V. Raghavan, *Crit. Rev. Food Sci. Nutr.*, 2022, **62**, 6446–6466.
4 R. Zhou, A. Rezaeimotlagh, R. Zhou, T. Zhang, P. Wang, J. Hong, B. Soltani, A. Mai-Prochnow, X. Liao, T. Ding, T. Shao, E. W. Thompson, K. Ostrikov and P. J. Cullen, *Trends Food Sci. Technol.*, 2022, **120**, 59–74.
5 K. Priya, N. Thirunavookarasu, D. V. Chidanand and J. Agric, *Food Res.*, 2023, **12**, 100623.
6 D. M. Lieu, T. T. K. Dang and H. T. Nguyen, *Food Chem. X*, 2025, **27**, 102388.
7 J. Wu, L. Zhang and K. Fan, *Crit. Rev. Food Sci. Nutr.*, 2024, **64**, 3823–3838.
8 F. Ye, M. Miao, K. Lu, B. Jiang, X. Li and S. W. Cui, *Food Hydrocoll.*, 2017, **67**, 37–44.
9 J. N. BeMiller and R. L. Whistler, *Starch: Chemistry and Technology*, Academic Press, 2009.
10 G. P. Singh, K. Aayush, P. Chavan, I. Chiu, S. Yan, R. Verma, K. Kuca, D. Kumar and T. Yang, *Innov. Food Sci. Emerg. Technol.*, 2024, **95**, 103722.
11 F. Wang, R. Ma and Y. Tian, *Food Chem.*, 2022, **382**, 132269.
12 R. I. Barbhuiya, C. Wroblewski, S. P. Ravikumar, J. Subramanian, A. Elsayed and A. Singh, *Foods*, 2025, **14**, 1860.
13 A. Hethnawi, R. Rajabi, A. M. Badran and Y. Tomazei, *Colloids Surf. A Physicochem. Eng. Asp.*, 2023, **674**, 131854.
14 S. Kumari, B. S. Yadav and R. B. Yadav, *Food Res. Int.*, 2020, **128**, 108765.
15 Z. Lin, H. Liu, J. J. Richardson, W. Xu, J. Chen, J. Zhou and F. Caruso, *Chem. Soc. Rev.*, 2024, **53**, 10800–10826.
16 D. Li, X. Xu, X. Wang, R. Li, C. Cai, T. Sun, Y. Zhao, L. Chen, J. Xu and N. Zhao, *ACS Appl. Nano Mater.*, 2019, **2**, 3510–3517.
17 Y. Guo, Q. Sun, F.-G. Wu, Y. Dai and X. Chen, *Adv. Mater.*, 2021, **33**, 2007356.
18 L. Huang, Q. Li, Q. Li, Y. Chi, Z. Xu and B. Shi, *J. Agric. Food Chem.*, 2025, **73**, 16064–16084.
19 J. Guo, Y. Ping, H. Ejima, K. Alt, M. Meissner, J. J. Richardson, Y. Yan, K. Peter, D. von Elverfeldt, C. E. Hagemeyer and F. Caruso, *Angew. Chem., Int. Ed.*, 2014, **53**, 5546–5551.
20 Q. Wang, Z. Rao, Y. Chen, L. Jiang, X. Lei, J. Zhao, F. Li, L. Lei and J. Ming, *Food Chem.*, 2024, **430**, 137025.
21 Y. Qin, J. Wang, C. Qiu, Y. Hu, X. Xu and Z. Jin, *ACS Sustain. Chem. Eng.*, 2019, **7**, 17379–17389.
22 X. Wang, T. Lan, M. Jin, Y. Dong, J. Shi, Z. Xu, L. Jiang, Y. Zhang and X. Sui, *Food Hydrocoll.*, 2023, **144**, 109019.
23 R. Jittham, N. Putdon, H. Uyama, Y.-I. Hsu, S. Theerakulpisut, M. Okhawilai, N. Srikhao and P. Kasemsiri, *Int. J. Biol. Macromol.*, 2025, **307**, 141774.
24 K. Xu, H. Li, X. Huang and Z. Qin, *Int. J. Biol. Macromol.*, 2022, **223**, 1462–1473.
25 J. H. Park, S. Choi, H. C. Moon, H. Seo, J. Y. Kim, S.-P. Hong, B. S. Lee, E. Kang, J. Lee, D. H. Ryu and I. S. Choi, *Sci. Rep.*, 2017, **7**, 6980.
26 S. Mao, Y. Zeng, Y. Ren, X. Ye and J. Tian, *Food Hydrocoll.*, 2025, **160**, 110722.
27 M. Ebrahimi, R. Karimi and A. D. Garmakhany, *Heliyon*, 2024, **10**, e23945.
28 X. Cheng, Y. Zhou, Z. Huo, R. Li, S. Xu, H. Qi, J. Zhu, F. Wang and Y. Bi, *Future Foods*, 2025, **12**, 100703.
29 A. Conde, F. Soares, R. Breia and H. Gerós, *Food Res. Int.*, 2018, **105**, 261–270.
30 Y. Chen, Z. Li, F. Ettoumi, D. Li, L. Wang, X. Zhang, Q. Ma, Y. Xu, L. Li, B. Wu and Z. Luo, *J. Hazard. Mater.*, 2022, **439**, 129685.
31 T. M. Pfukwa, O. A. Fawole, M. Manley, P. A. Gouws, U. L. Opara and C. Mapiye, *Sustainability*, 2019, **11**, 1746.

32 Y. Qin, J. Wang, C. Qiu, Y. Hu, X. Xu and Z. Jin, *ACS Sustain. Chem. Eng.*, 2019, **7**, 17379–17389.
33 A. R. da Silva Bruni, E. da Silva Alves, J. C. M. da Costa, J. de S. A. Friedrichsen, L. G. Z. Silva, O. de Oliveira Santos Junior and E. G. Bonafé, *ACS Food Sci. Technol.*, 2024, **4**, 2967–2979.
34 R. Mandal, A. Wiktor, X. Mohammadi and A. Pratap-Singh, *Food Bioprocess Technol.*, 2022, **15**, 92–104.
35 Y. Jiang and C. Li, *PLoS One*, 2015, **10**, e0121969.
36 J. Chetia, P. Adhikary, L. M. Devi and L. S. Badwaik, *Sustain. Chem. Pharm.*, 2023, **32**, 101034.
37 I. L. Lawag, E. S. Nolden, A. A. M. Schaper, L. Y. Lim and C. Locher, *Appl. Sci.*, 2023, **13**, 2135.
38 C. Luo, F. Xie, Q. Chen, J. Zhou, Z. He and J. Cai, *Food Chem.*, 2025, **467**, 142203.
39 K. Sridhar and A. L. Charles, *Food Chem.*, 2019, **275**, 41–49.
40 H. Yong, H. Hu, Z. Wang, D. Yun, J. Kan and J. Liu, *J. Sci. Food Agric.*, 2022, **102**, 6373–6386.
41 F.-X. Xiao, M. Pagliaro, Y.-J. Xu and B. Liu, *Chem. Soc. Rev.*, 2016, **45**, 3088–3121.
42 M. Danaei, M. Dehghankhold, S. Ataei, F. Hasanzadeh Davarani, R. Javanmard, A. Dokhani, S. Khorasani and M. R. Mozafari, *Pharmaceutics*, 2018, **10**, 57.
43 N. Andrikopoulos, Y. Li, A. Nandakumar, J. F. Quinn, T. P. Davis, F. Ding, N. Saikia and P. C. Ke, *ACS Appl. Mater. Interfaces*, 2023, **15**, 7777–7792.
44 X. Hu, T. Ma, H. Pan, S. Chen and D. Liu, *Food Res. Int.*, 2025, **214**, 116625.
45 N. Sizochenko, A. Mikolajczyk, M. Syzochenko, T. Puzyn and J. Leszczynski, *NanoImpact*, 2021, **22**, 100317.
46 R. Lufu, A. Ambaw and U. L. Opara, *Postharvest Biol. Technol.*, 2019, **157**, 110982.
47 H. Congying, W. Meifang, Md. N. Islam, S. Cancan, G. Shengli, A. Hossain and C. Xiaohuang, *J. Food Process. Preserv.*, 2024, **48**, e3026836.
48 J. Xu, Q. Wang, J. Yu, S. Yan and B. Qi, *Food Hydrocoll.*, 2024, **156**, 110309.
49 H. Aloui, K. Khwaldia, L. Sánchez-González, L. Muneret, C. Jeandel, M. Hamdi and S. Desobry, *Int. J. Food Sci. Technol.*, 2014, **49**, 952–959.
50 X. Huang, M. Hong, L. Wang, Q. Meng, Q. Ke and X. Kou, *Food Hydrocoll.*, 2023, **136**, 108255.
51 S. R. Roberto, A. M. de Assis, L. Y. Yamamoto, L. C. V. Miotto, A. J. Sato, R. Koyama and W. Genta, *Sci. Hortic.*, 2012, **142**, 44–48.
52 V. Jamali, A. Emamifar, H. Beiginejad, M. Moradi and M. Rasouli, *J. Food Meas. Charact.*, 2024, **18**, 9959–9970.
53 C. Tyl, G. D. Sadler, in *Food Analysis*, ed. S. S. Nielsen, Springer International Publishing, Cham, 2017, pp. 389–406.
54 I. Baccichet, R. Chiozzotto, D. Bassi, C. Gardana, M. Cirilli and A. Spinardi, *Sci. Hortic.*, 2021, **278**, 109865.
55 K. Yu, L. Yang, S. Zhang, N. Zhang, D. Zhu, Y. He, X. Cao and H. Liu, *Food Chem.*, 2025, **468**, 142513.
56 S. Wang, J. Tang, M. Liu, F. Meng, S. Wang, Y. Bai, H. Zhou and K. Du, *Food Biosci.*, 2024, **62**, 105572.
57 J. Hu, X. Wang, Q. Sun, S. Yang, M. Feng, T. Zhang and H. Hong, *Adv. Funct. Mater.*, 2025, **35**, 2416918.
58 C. Pucci, C. Martinelli, D. De Pasquale, M. Battaglini, N. di Leo, A. Degl'Innocenti, M. B. Gümüş, F. Drago and G. Ciofani, *ACS Appl. Mater. Interfaces*, 2022, **14**, 15927–15941.
59 J. Zhao, D. Qian, L. Zhang, X. Wang and J. Zhang, *RSC Adv.*, 2024, **14**, 10410–10415.
60 M. Kowczyk-Sadowy, R. Świsłocka, H. Lewandowska, J. Piekut and W. Lewandowski, *Molecules*, 2015, **20**, 3146–3169.
61 Z. Chen, R. Świsłocka, R. Choińska, K. Marszałek, A. Dąbrowska, W. Lewandowski and H. Lewandowska, *Int. J. Mol. Sci.*, 2024, **25**, 11775.
62 J. A. Lemire, J. J. Harrison and R. J. Turner, *Nat. Rev. Microbiol.*, 2013, **11**, 371–384.
63 H.-T. Zheng, H. L. Bui, S. Chakroborty, Y. Wang and C.-J. Huang, *Langmuir*, 2019, **35**, 8829–8839.
64 W.-R. Diao, Q.-P. Hu, S.-S. Feng, W.-Q. Li and J.-G. Xu, *J. Agric. Food Chem.*, 2013, **61**, 6044–6049.
65 S. Chiera, F. Bosco, C. Mollea, A. Piscitello, R. Sethi, G. Nollo, I. Caola and F. Tessarolo, *Sci. Rep.*, 2023, **13**, 21807.
66 S. Wardejn, S. Wacławek and G. Dudek, *Int. J. Mol. Sci.*, 2024, **25**, 12580.